Self-consistent random-phase approximation for interacting electrons in quantum wells and intersubband absorption

Sergey V. Faleev[1,2] and Mark I. Stockman[1,*]
[1]*Department of Physics and Astronomy, Georgia State University, Atlanta, Georgia 30303*
[2]*Sandia National Laboratories, Livermore, California 94551*
(Received 23 September 2001; revised manuscript received 1 February 2002; published 20 August 2002)

For electrons with Coulomb interaction confined in a quantum well, we have developed an approach based on the Kadanoff-Baym-Keldysh technique to calculate equilibrium Green's functions. This approach is based on iterative numerical computation of the retarded self-energy in the self-consistent random-phase approximation. For two subbands, at zero temperature, we have computed spectral functions, electron distributions, quasiparticle spectra, and the current-current correlation function that determines the intersubband absorption coefficient. Our computations of the optical absorption take into account the depolarization shift and vertex corrections. Apart from direct applications of this theory to the physics of semiconductor quantum well devices, the Green's functions obtained may also serve as self-consistent initial conditions for quantum kinetics problems in quantum wells.

DOI: 10.1103/PhysRevB.66.085318 PACS number(s): 73.21.−b, 05.30.Fk, 78.67.−n

I. INTRODUCTION

Intersubband absorption of electrons in quantum wells is among the most important properties from both fundamental and applied positions. In particular, one of the most developed and frequently used applications of quantum wells is quantum-well infrared photodetectors (see, e.g., Refs. 1–3). For this application, and many others, electron densities are high enough in order to yield sufficiently high responses. Consequently, significant effects of many-body electron-electron interaction are present in the intersubband absorption (see, e.g., Sec. 2.7.2 in Ref. 1 and Chap. 4 in Ref. 2). The intersubband absorption is also of high significance for another important application of quantum wells, namely, quantum cascade lasers.[4] In this paper, we develop a theory of intersubband absorption based on the fully self-consistent random-phase approximation (also known as the *GW* approximation), and apply it to intersubband absorption in specific quantum-well infrared photodetectors.

Another perspective application of the present results is the description of an initial correlated electron state for ultrafast physics. Stimulated by the development of ultrashort laser pulses, theoretical and experimental studies of ultrafast kinetics of interacting electrons in semiconductors have experienced rapid development. This problem is very interesting and theoretically complicated due to the fact that *many-body* Coulomb interaction on a very short time scale is not efficiently screened and therefore is very strong.[5–13] From the applied point of view, the research on the ultrafast kinetics promises important contributions to the physics of ultrafast electronic and optoelectronic devices. Significant theoretical progress in this field has recently been obtained on the basis of the nonequilibrium Green's-function method by Kadanoff and Baym[14] and Keldysh.[15] This method has been further developed by Langreth[16] and Rammer and Smith.[17]

It is widely recognized that the conventional equilibrium field-theoretical technique (described, e.g., in Ref. 18) is not applicable to the ultrafast kinetic problems where the Kadanoff-Baym-Keldysh (KBK) method of nonequilibrium Green's-functions is valid and should be used. However, it is much less appreciated that the equilibrium Green's-function method may also not be applicable to the interaction of light with many-body systems, because this method is based on an adiabatic switching-on the interactions, while, in contrast, the light field is rapidly oscillating. Therefore, even for the continuous-wave (cw) excitation of many-electron systems, the nonequilibrium KBK approach may be necessary. The KBK method also has an added advantage that the initial (equilibrium) electron system can be conveniently treated at a given finite temperature.

It is necessary to mention that there has been a significant amount of work done in the field of interacting electrons using the well-known semiconductor Bloch equations (SBE's) (see, e.g., Ref. 19). In contrast to the two-time KBK equations, the SBE's are single-time equations that can be obtained from the KBK equations by using additional approximations. In particular, they can be derived from the KBK equations using the generalized Kadanoff-Baym ansatz (see, e.g., Ref. 20) whose accuracy is not quite controllable. This ansatz cannot be derived consistently microscopically and expressed as a result of a summation of some subset of contributions (diagrams). Some additional approximations such as use of the zero-order retarded and advanced Green's functions also are invoked.[20]

In the present paper, we consider intersubband optical absorption for the electrons in the conduction band of a quantum well. As the necessary first stage of this project and of separate interest, we find equilibrium many-body Green's functions of the electrons in the quantum well, taking into account the two lowest subbands. The KBK technique used by us provides a unified and powerful method of solving both these problems, equilibrium and nonequilibrium (optical). As we already mentioned above, the equilibrium Green's functions of the KBK theory, that we have determined in this research, can also be used as initial conditions in the future studies on ultrafast intersubband kinetics of interacting electrons in quantum wells.

Because it is impossible to exactly solve the many-electron Coulomb-interaction problem, one has to resort to approximations. The random phase approximation (RPA) is

 ©2002 The American Physical Society

the most widely used and realistic approximation for many-body electron problems. Of principal importance is that for the quantum kinetics problems and, generally, for optical excitation problems, the RPA should *necessarily* be self-consistent (SC), otherwise the local conservation laws for the electron density and energy-momentum density are violated.[21] The self-consistency of the RPA means that Green's functions that are employed to calculate the polarization operator in the "bubble" approximation $\Pi = GG$ and the self-energy in the GW approximation $\Sigma = GW$ are the final Green's functions that satisfy the Dyson equation with self-energy Σ. Note that the theories such as SCRPA that are compatible with the exact conservation laws are called conserving.[21] In this respect we note that some theories do not employ a completely self-consistent approximation and, therefore, are not necessarily conserving. As an example, we mention Ref. 22 by Barth and Holm, which is a GW_0 theory, which means that the self-energy Σ is calculated with the final Green's functions G, but the screened (renormalized) interaction is calculated with the non-self-consistent Green's functions G_0. In contrast, a later paper[23] by the same authors was the first, to our knowledge, example of the application of a fully self-consistent RPA (GW approximation), which is conserving, to a 3D electron gas.

Taking into account the above-discussed compelling arguments, we earlier employed the SCRPA in the framework of the KBK approach to find the Green's function and various observable quantities, such as the momentum distribution, one-electron energy, spectral function, etc., of a two-dimensional (2D) electron gas at the zero and finite temperatures.[24,25] In the present study, we generalize this approach to describe the state and optical absorption of electrons in the conduction subband of a quantum well. Previously, a significant number of theoretical papers were devoted to a computation of the intersubband absorption (see, e.g., Refs. 26–29). These theories are based on different versions of the RPA, but none of them, distinct from the present theory, is a SCRPA. In qualitative agreement with previous results,[26,27] we found a significant depolarization blueshift of the absorption spectrum maximum. However, quantitatively, the self-consistency of the RPA leads to an increase of the total blueshift compared with the usual (non-self-consistent) RPA. We have also evaluated the vertex corrections in the current-current correlation function using the ladder approximation. These corrections result in a small increase of the magnitude of the absorption peak, with an almost nondistinguishable redshift in the peak position.

This paper is organized in the following way. In Sec. II we present general equations and their solutions for Green's functions and optical absorption. Numerical procedures are described in Sec. III. The results of numerical computations are presented in Sec. IV. Finally, concluding remarks are given in Sec. V.

II. THEORY AND BASIC EQUATIONS

A. Green's functions

We consider an electron system with the Coulomb interaction confined in quantum well with two subband states. The positive ions are described by a jellium model. The Hamiltonian of the system is

$$H=\sum_{i,\mathbf{p}} (E^{(0)}_{i,\mathbf{p}}-\mu)a^{\dagger}_{i,\mathbf{p}}a_{i,\mathbf{p}} + \frac{1}{2S}\sum_{i,j,k,l,\mathbf{q},\mathbf{p},\mathbf{p}'} V_{ijkl}(\mathbf{q})a^{\dagger}_{i,\mathbf{p}+\mathbf{q}}a^{\dagger}_{j,\mathbf{p}'-\mathbf{q}}a_{k,\mathbf{p}'}a_{l,\mathbf{p}}, \quad (1)$$

where S is the area of the quantum well, μ is the chemical potential; $\mathbf{p}$, $\mathbf{p}'$, and $\mathbf{q}$ are 2D momentum vectors in the plane of the well, indexes $i,j,k,l=1,2$ denote the subband (envelope) states whose wave functions are $\phi_1(z)$ and $\phi_2(z)$, with z as the growth direction (i.e., the normal to the well plane); and $E^{(0)}_{1,\mathbf{p}}=p^2/2m$ and $E^{(0)}_{2,\mathbf{p}}=p^2/2m+E^{(0)}_{12}$ are one-particle energies, where $E^{(0)}_{12}$ is the bare energy gap and m is the bare effective mass of the electron. The original (unscreened) Coulomb potential is given by the usual expression

$$V_{ijkl}(\mathbf{q})=\int dz\,dz'\,\phi^*_i(z)\phi^*_j(z')v(\mathbf{q},z-z')\phi_k(z')\phi_l(z), \quad (2)$$

where

$$v(\mathbf{q},z)=\int d^2\mathbf{r}e^{i\mathbf{q}\mathbf{r}}\frac{e^2}{\epsilon_b\sqrt{\mathbf{r}^2+z^2}}=\frac{2\pi e^2}{\epsilon_b q}e^{-q|z|}.$$

ϵ_b is the background dielectric constant, and e is the electron charge.

The subband wave functions in the absence of a magnetic field can be chosen real, so the potential V_{ijkl} of Eq. (2) has the following permutation symmetry: $V_{ijkl}=V_{ljki}=V_{ikjl}=V_{jilk}$. In the following we assume that the well is symmetric with respect to its middle ($z=0$); therefore the wave functions have a definite parity: $\phi_1(-z)=\phi_1(z)$ and $\phi_2(-z)=-\phi_2(z)$. In this case, only four independent matrix elements of V_{ijkl} do not vanish, which we denote $V_1(\mathbf{q})\equiv V_{1111}(\mathbf{q})$, $V_2(\mathbf{q})\equiv V_{2222}(\mathbf{q})$, $V_c(\mathbf{q})\equiv V_{1221}(\mathbf{q})$, and $V_x(\mathbf{q})\equiv V_{1212}(\mathbf{q})$.

The Kadanoff-Baym (KB) equations are formulated for a set of four Green's functions: greater $G^>$, lesser $G^<$, retarded G^r, and advanced G^a. Similar notations are used for the components of other field-theoretical objects, such as the self-energy Σ, polarization operator Π, dynamically-screened interaction W, etc.

We deal with equilibrium uniform systems where the Green's functions depend only on a conserving momentum $\mathbf{p}$ and time difference t, and are defined in the momentum-time representation as

$$G^<_i(\mathbf{p},t)=i\langle a^{\dagger}_{i,\mathbf{p}}(0)a_{i,\mathbf{p}}(t)\rangle,$$

$$G^>_i(\mathbf{p},t)=-i\langle a_{i,\mathbf{p}}(t)a^{\dagger}_{i,\mathbf{p}}(0)\rangle, \quad (3)$$

where the angular brackets denote quantum-mechanical averaging *and* averaging over the Gibbs ensemble; we do not show the spin indices over which all objects are diagonal. Also, the equilibrium Green's functions are diagonal over subband indexes due to conserved parity in the absence of external electrical field.

For any object $\mathcal{A}$ of the theory (the Green's function G, self-energy Σ, dynamically screened potential W, polarization operator Π, etc.), the corresponding retarded (r) and advanced (a) components are expressed as

$$\mathcal{A}^{r,a}(\mathbf{p},t)=\pm\theta(\pm t)[\mathcal{A}^{>}(\mathbf{p},t)-\mathcal{A}^{<}(\mathbf{p},t)]+\delta(t)\mathcal{A}^{s}, \quad (4)$$

where the second (singular in time) term $\delta(t)\mathcal{A}^s$ is not related to $\mathcal{A}^{>,<}$, and appears due to concatenation of regular objects with time-singular quantities such as potentials that do not include retardation [see, e.g., the second integral in the right-hand side of Eq. (23)]. From the four types (components) of each quantity, only three are independent due to an identity

$$\mathcal{A}^{r}-\mathcal{A}^{a}=\mathcal{A}^{>}-\mathcal{A}^{<}. \quad (5)$$

In a stationary case, there is a symmetry relation between the advanced and retarded components of an object in the momentum-frequency representation:

$$\mathcal{A}^{a*}(\mathbf{p},\omega)=\mathcal{A}^{r}(\mathbf{p},\omega). \quad (6)$$

Also, the well known Kubo-Martin-Schwinger boundary condition is valid,[17]

$$G_i^{>}(\mathbf{p},\omega)=-\exp(\beta\omega)G_i^{<}(\mathbf{p},\omega), \quad (7)$$

where $\beta=1/T$ and T is temperature in energy units. Using this relation, the number of independent components can be reduced to only one. We choose G^r as such an independent component, and the other three are expressed as

$$G_i^{a}(\mathbf{p},\omega)=G_i^{r*}(\mathbf{p},\omega)$$

$$G_i^{<}(\mathbf{p},\omega)=-i2n_{\omega}\mathrm{Im}[G_i^{r}(\mathbf{p},\omega)],$$

$$G_i^{>}(\mathbf{p},\omega)=-i2(n_{\omega}-1)\mathrm{Im}[G_i^{r}(\mathbf{p},\omega)], \quad (8)$$

where $n_{\omega}=[\exp(\omega/T)+1]^{-1}$ is the Fermi factor, and we use a system of units where $\hbar=1$.

We use an iterative process to find Green's function G^r numerically. As the result of an iterative step, we obtain the retarded self-energy $\Sigma_i^r(\mathbf{p},\omega)$. The following is a description of the next iterative step.

Using the Dyson equation for the retarded Green's function, we find

$$G_i^{r}(\mathbf{p},\omega)=\frac{1}{\omega-\xi_{i,\mathbf{p}}-\Sigma_i^{r}(\mathbf{p},\omega)}, \quad (9)$$

where $\xi_{i,\mathbf{p}}=E_{i,\mathbf{p}}^{(0)}-\mu$, and $i=1,2$. From this, using Eqs. (8), we find $G^{>,<}$. This allows us to obtain the electron polarization operator in the RPA (bubble) approximation $\Pi=GG$, or in the detailed form

$$\Pi_{ij}^{<}(\mathbf{p},\omega)=-2i\int\frac{d\omega' d^2\mathbf{k}}{(2\pi)^3}G_i^{<}(\mathbf{k},\omega')G_j^{>}(\mathbf{k}-\mathbf{p},\omega'-\omega), \quad (10)$$

where we used the known Langreth rules for the concatenation of two Green's functions.[16] From this, using Eqs. (5) and (6) and the symmetry relation

$$\Pi_{ij}^{>}(\mathbf{p},\omega)=\Pi_{ji}^{<}(\mathbf{p},-\omega), \quad (11)$$

we compute the imaginary part of the retarded polarization operator:

$$\mathrm{Im}\Pi_{ij}^{r}(\mathbf{p},\omega)=\frac{1}{2i}[\Pi_{ji}^{<}(\mathbf{p},-\omega)-\Pi_{ij}^{<}(\mathbf{p},\omega)]. \quad (12)$$

Because $\Pi_{ij}^r(\mathbf{p},\omega)$ as a function of ω is analytical and has no singularities in the upper half plane, and it tends to zero for $\omega\to\infty$, the conventional Kramers-Kronig relation allows one to restore its real part,

$$\mathrm{Re}\Pi_{ij}^{r}(\mathbf{p},\omega)=\frac{1}{\pi}\mathrm{P}\int d\omega'\frac{\mathrm{Im}\Pi_{ij}^{r}(\mathbf{p},\omega')}{\omega'-\omega}, \quad (13)$$

where P denotes the principal value of the integral.

Having found the retarded components of the polarization operator, we write down the system of Dyson equations for the retarded dynamically screened potentials $W_1(\mathbf{p},\omega)$, $W_2(\mathbf{p},\omega)$, $W_c(\mathbf{p},\omega)$, and $W_x(\mathbf{p},\omega)$:

$$W_1^r=V_1+V_1\Pi_{11}^rW_1^r+V_c\Pi_{22}^rW_c^r,$$

$$W_2^r=V_2+V_2\Pi_{22}^rW_2^r+V_c\Pi_{11}^rW_c^r,$$

$$W_c^r=V_c+V_1\Pi_{11}^rW_c^r+V_c\Pi_{22}^rW_2^r,$$

$$W_x^r=V_x+V_x(\Pi_{12}^r+\Pi_{21}^r)W_x^r. \quad (14)$$

These Dyson equations describe the ''dressing'' of the bare potentials $V_1(\mathbf{p})$, $V_2(\mathbf{p})$, $V_c(\mathbf{p})$, and $V_x(\mathbf{p})$ by the chains of corresponding polarization operators. Here and below, we use the known Langreth rules[16] that allow one to find components of the product of two objects $\mathcal{A}$ and $\mathcal{B}$;

$$(\mathcal{AB})^{r,a}=\mathcal{A}^{r,a}\mathcal{B}^{r,a}, \quad (\mathcal{AB})^{>,<}=\mathcal{A}^{>,<}\mathcal{B}^{a}+\mathcal{A}^{r}\mathcal{B}^{>,<}. \quad (15)$$

The solutions of Eqs. (14) are

$$W_1^r=\left[V_1+\frac{V_c^2\Pi_2^r}{(1-V_1\Pi_1^r)(1-V_2\Pi_2^r)-V_c^2\Pi_1^r\Pi_2^r}\right]\frac{1}{1-V_1\Pi_1^r},$$

$$W_2^r=\left[V_2+\frac{V_c^2\Pi_1^r}{(1-V_1\Pi_1^r)(1-V_2\Pi_2^r)-V_c^2\Pi_1^r\Pi_2^r}\right]\frac{1}{1-V_2\Pi_2^r},$$

$$W_c^r=\frac{V_c}{(1-V_1\Pi_1^r)(1-V_2\Pi_2^r)-V_c^2\Pi_1^r\Pi_2^r},$$

$$W_x^r=\frac{V_x}{1-V_x(\Pi_{12}^r+\Pi_{21}^r)}, \quad (16)$$

where we used notations $\Pi_1\equiv\Pi_{11}$ and $\Pi_2\equiv\Pi_{22}$ for brevity.

Using Eqs. (7) and (10), one can derive a relation for the greater and lesser components of the polarization operators, analogous to the relation for Green's functions (7):

$$\Pi_{ij}^{>}(\mathbf{p},\omega)=\exp(\beta\omega)\Pi_{ij}^{<}(\mathbf{p},\omega). \tag{17}$$

In general, this relation can be proved in the same way as the Kubo-Martin-Schwinger boundary condition.[17] Using this and applying the Langreth rules [Eq. (15] to the lesser and greater components of the renormalized potential W that is built from the multiple products of the polarization operators, one can derive that a similar relation is valid for each of the potentials W_1, W_2, W_c, and W_x:

$$W^{>}(\mathbf{p},\omega)=\exp(\beta\omega)W^{<}(\mathbf{p},\omega). \tag{18}$$

Combining Eqs. (5) and (6) for the renormalized Coulomb potential and using relation (18), we obtain the expression for the lesser component of the potential,

$$W^{<}(\mathbf{p},\omega)=\frac{2i}{e^{\beta\omega}-1}\,\mathrm{Im}\;W^{r}(\mathbf{p},\omega), \tag{19}$$

where W^r is given by Eq. (16). The greater component of the dynamically screened potential W can be obtained from symmetry relations

$$W^{>}(\mathbf{p},\omega)=W^{<}(\mathbf{p},-\omega),\quad W^{a}(\mathbf{p},\omega)=W^{r}(\mathbf{p},-\omega). \tag{20}$$

To complete the current iteration step, we compute the lesser and greater self-energies in the SCRPA (the GW approximation) as

$$\Sigma_i^{>,<}(\mathbf{p},\omega)=i\int\frac{d\omega' d^2\mathbf{k}}{(2\pi)^3}[W_i^{>,<}(\mathbf{k},\omega')G_i^{>,<}(\mathbf{p}-\mathbf{k},\omega-\omega') + W_x^{>,<}(\mathbf{k},\omega')G_{3-i}^{>,<}(\mathbf{p}-\mathbf{k},\omega-\omega')]. \tag{21}$$

Taking into account Eqs. (5) and (6), we can express the imaginary part of the retarded self-energy as

$$\mathrm{Im}\Sigma_i^{r}(\mathbf{p},\omega)=\frac{1}{2i}[\Sigma_i^{>}(\mathbf{p},\omega)-\Sigma_i^{<}(\mathbf{p},\omega)]. \tag{22}$$

Finally, $\mathrm{Re}\Sigma_i^r$ is found from a dispersion relation

$$\mathrm{Re}\Sigma_i^{r}(\mathbf{p},\omega)=\frac{1}{\pi}\mathrm{P}\int d\omega'\frac{\mathrm{Im}\Sigma_i^{r}(\mathbf{p},\omega')}{\omega'-\omega} -\int\frac{d^2\mathbf{k}}{(2\pi)^2}[V_i(\mathbf{k})n_i(\mathbf{p}-\mathbf{k}) + V_x(\mathbf{k})n_{3-i}(\mathbf{p}-\mathbf{k})], \tag{23}$$

where the momentum distribution function $n_i(\mathbf{p})$ for each subband is expressed as

$$n_i(\mathbf{p})=-i\int\frac{d\omega}{2\pi}G_i^{<}(\omega,\mathbf{p}). \tag{24}$$

The last integral in the right-hand side of Eq. (23) is the exchange diagram that is ω independent, yielding a correct asymptotic behavior of $\mathrm{Re}\Sigma_i^r(\mathbf{p},\omega)$ for $\omega\to\infty$.

Concluding this subsection, we have started with Σ_i^r [see the paragraph preceding, Eq. (9)] and finished with the next-iteration Σ_i^r [Eqs. (22) and (23)]. This closes the iterative procedure. All the necessary Green's function are self-consistently found within the current iteration [Eqs. (8) and (9)].

B. Intersubband linear absorption spectrum

The linear absorption coefficient $\alpha(\omega)$ is related by the Kubo formula to the imaginary part of retarded current-current correlation function $\pi^r(\omega)$,[32]

$$\alpha(\omega)=-\frac{4\pi}{\sqrt{\epsilon_b}V\omega}\,\mathrm{Im}\;\pi^{r}(\omega), \tag{25}$$

where V is the 3D volume of the system. This retarded current-current correlation function is given by

$$\pi^{r}(\omega)=|p_z|^2S\frac{\Pi_{21}^{r}(\mathbf{q}=0,\omega)}{1-V_x(\mathbf{q}=0)\Pi_{21}^{r}(\mathbf{q}=0,\omega)}, \tag{26}$$

where $p_z=(e/m)\int dz\,\phi_2(z)(d/dz)\phi_1(z)$ is the matrix element of the current between the two subbands, where we assume that the exciting light is linearly polarized in the growth (z) direction of the quantum well. In Eq. (26), we neglect the small Π_{12} polarization operator and retain only the Π_{21} polarization operator that describes the resonant absorption of the light when an electron undergoes the transition from subband 1 to subband 2, which is the well-known resonant or rotating-wave approximation. In the SCPRA ("bubble" approximation), the polarization operator Π_{21}^r is given by Eqs. (10)–(13). Note that Eq. (26) is applicable to both single and multiple quantum wells, where in the latter case V is the system's volume per one quantum well.

To go beyond the "bubble" approximation, we need to calculate corrections to the vertex $\Gamma(\mathbf{p},\omega')$. We use the ladder approximation which is the most common approximation for the vertex corrections. To study the vertex corrections to the polarization operator, we present this operator as the concatenation of the intersubband (nondiagonal over subband indices) Green's function G_{21} in the presence of an electromagnetic field with frequency ω,

$$\Pi_{21}^{r}(\mathbf{q}=0,\omega)=-2i\int\frac{d\omega' d^2\mathbf{p}}{(2\pi)^3}G_{21}^{<}(\mathbf{p},\omega+\omega',\omega'), \tag{27}$$

where this intersubband Green function G_{21} is related to the vertex Γ as

$$G_{21}(\mathbf{p},\omega+\omega',\omega')=G_2(\mathbf{p},\omega+\omega')\Gamma(\mathbf{p},\omega+\omega',\omega')\times G_1(\mathbf{p},\omega'). \tag{28}$$

We exclude the matrix element of the current from the vertex, so the pure SCRPA corresponds to $\Gamma=1$. In Eq. (27), the

retarded component of the polarization operator is related to the *lesser* component of the intersubband Green's function because the Langreth rule[16] for the retarded component of two operators concatenated into a loop are exactly the same as for the lesser component of product of these two operators in Eq. (15).

We use an iterative process to find the intersubband Green's function $G_{21}(\mathbf{p},\omega')$ numerically for each light frequency ω independently. As the result of an iterative step, we obtain three components of the vertex function $\Gamma^{<,r,a}(\mathbf{p},\omega')$. The following is the description of the next iterative step.

Using the Langreth rules of Eqs. (15) and (28), we can determine the components of the G_{21} functions

$$G_{21}^{r,a}=G_2^{r,a}\Gamma^{r,a}G_1^{r,a},$$

$$G_{21}^{<}=G_2^{r}\Gamma^{r}G_1^{<}+G_2^{r}\Gamma^{<}G_1^{a}+G_2^{<}\Gamma^{a}G_1^{a}. \tag{29}$$

Note that in contrast to Eq. (6), the retarded and advanced components of the Green's function G_{21} are not related by complex conjugation [in fact, $(G_{12}^{r})^{*}=G_{21}^{a}$].

To complete the iteration cycle, we calculate the vertex function Γ in the ladder approximation, where it satisfies the equations

$$\Gamma^{<}(\mathbf{p},\omega+\omega',\omega')=i\int\frac{d\omega''d^2\mathbf{k}}{(2\pi)^3}G_{21}^{<}(\mathbf{k},\omega+\omega'',\omega'')W_c^{<}(\mathbf{p}-\mathbf{k},\omega'-\omega''),$$

$$\Gamma^{r,a}(\mathbf{p},\omega+\omega',\omega')=1+i\int\frac{d\omega''d^2\mathbf{k}}{(2\pi)^3}[G_{21}^{r,a}(\mathbf{k},\omega+\omega'',\omega'')\times W_c^{<}(\mathbf{p}-\mathbf{k},\omega''-\omega')+G_{21}^{<}(\mathbf{k},\omega+\omega'',\omega'')W_c^{r,a}(\mathbf{p}-\mathbf{k},\omega'-\omega'')], \tag{30}$$

where we used the relations of Eq. (20) for the greater component of the potential $W^{>}$.

III. NUMERICAL PROCEDURES

A. Numerical procedures for Green's functions in equilibrium

We have numerically solved the equations for the Green's function in equilibrium using the iterative procedure described above in Sec. II A. Though these equations are valid for arbitrary temperatures, in this paper we have performed computations for $T=0$. Our motivation for this choice is that we intend to concentrate on effects of Coulomb interaction for electrons in a quantum well with two subbands taken into account. A finite temperature will bring about additional effects that will be considered elsewhere. Also, the previous RPA calculations for intersubband absorption spectra,[26,27] with which we compare, were carried out at $T=0$.

We choose the confining well potential to be zero in the well region, $z\in(-d/2,d/2)$, and infinite elsewhere. Thus the ground-state and first-exited-state wave functions are

$$\phi_1(z)=\sqrt{2/d}\,\cos(\pi z/d),\quad \phi_2(z)=\sqrt{2/d}\,\sin(2\pi z/d), \tag{31}$$

where the width d of the well is related to the bare intersubband gap $E_{12}^{(0)}$ as $d=\sqrt{3/(2mE_{12}^{(0)})}$. Using these wave functions, the integrals of Eq. (2) are easily calculated analytically.

The final electron density of the system is controlled by the chemical potential μ. One can convince oneself that all dimensionless quantities of the theory depend only on two dimensionless parameters $r_s^0\equiv e^2\sqrt{m|\mu|}/(\epsilon_b\mu)$ and $E_{12}^{(0)}/|\mu|$. Note that for interacting electrons, the chemical potential is not necessarily positive. Alternatively, it is convenient to present the results as functions of two ''dressed'' dimensionless parameters: a conventional density parameter (that is the relative distance between electrons) r_s and a relative bare intersubband gap $\rho=E_{12}^{(0)}/\varepsilon_F$. For a 2D electron gas, $r_s\equiv me^2/\epsilon_b\sqrt{\pi n}$, where $n=2\Sigma_i\int n_i(\mathbf{p})d^2\mathbf{p}/(2\pi)^2$ is the electron density. The Fermi energy ε_F is conventionally related to the Fermi momentum p_F at which the discontinuity in the electron momentum distribution occurs: $\varepsilon_F\equiv p_F^2/(2m)$.

In the numerical integrations in Eqs. (10), (13), (21), (23), and (24), the integration over the momentum variables has been truncated at the maximum momentum p_{max} that is (depending on the r_s^0) from 6–10 times the Fermi momentum p_F. The frequency (energy) integrations were carried out within the region $|\omega|<p_{max}^2/m$.

We ran the iterative procedure described above in Sec. II A until the self-energies $\Sigma_i^r(\mathbf{p},\omega)$ converged (uniformly in $\mathbf{p}$ and ω) within $\leqslant 1\%$ mismatch. This requires about 15 iterations and takes ≈ 100 h of CPU time on an SGI Origin 2000 workstation. This iterative procedure has been well-converging and stable. We found earlier for a 2D electron gas[24,25] that such an iterative procedure converged for $r_s\leqslant 2.62$; the values used in this paper are well within this range. As the initial self-energy we have used either the result[24] of a pure 2D case with the same value of r_s^0 for $\Sigma_1^r(\mathbf{p},\omega)$ and a small constant value for $\Sigma_2^r(\mathbf{p},\omega)$, or the result of a previous SCRPA run with a different value of r_s^0. There was no appreciable dependence of the final results on the initial value of $\Sigma_i^r(\mathbf{p},\omega)$, implying a good convergence.

Integrating over the angle between $\mathbf{p}$ and $\mathbf{k}$ and over ω', we divided the integration interval into 20–40 segments to take advantage of the smooth behavior of the integrands in some segments. The number of segments was chosen to optimize the computational efficiency. The adaptive Romberg integration of fifth-order accuracy was used to integrate over each of these segments. This method allowed us to achieve a relative error of integration of less than 10^{-4}. We computed the self-energies and polarization operators in 200–400 points in their arguments p and ω. We verified that the results obtained are stable and do not depend appreciably on any of the computational parameters mentioned above within their indicated range.

B. Numerical procedures for optical absorption including vertex corrections

In the integrals in Eqs. (30), a numerical integration was performed following a numerical procedure similar to that

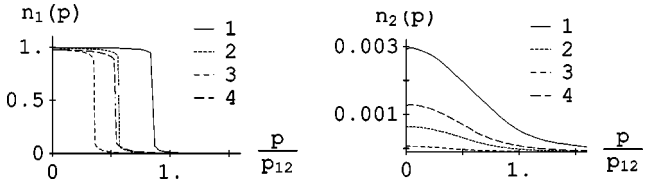

FIG. 1. Electron momentum distributions for the first and second subbands, $n_1(p)$ and $n_2(p)$, calculated in the SCRPA approximation. Curves 1–4 correspond to the pairs of parameters: $\{r_s,\rho\}=\{0.7,1.35\}$, $\{1.06,3.13\}$, $\{1.69,7.85\}$, and $\{2.17,3.46\}$.

described in Sec. III A. We ran the iterations of Eqs. (29) and (30) until the intersubband Green's functions $G_{21}^{r,a,<}(\mathbf{p},\omega+\omega',\omega')$ converged (uniformly in $\mathbf{p}$ and ω) within $a\leqslant 1\%$ mismatch. This convergence is very fast, and it requires only from 2–4 iterations to achieve the required accuracy. Each iteration takes typically ≈ 10 h of CPU time on an SGI Origin 2000 workstation for each point in light frequency ω. We have used eight processors in parallel to find G_{21} in different points over ω.

As the initial Γ we used either $\Gamma=1$ or the result of a previous run with a different value of ω. There was no appreciable dependence of the final results on the initial values of $\Gamma^{r,a,<}(\mathbf{p},\omega+\omega',\omega')$, signifying a good convergence.

IV. NUMERICAL RESULTS

A. Equilibrium electron properties

The momentum distributions $n_i(p)$ for electrons in each subband ($i=1,2$) are shown in Fig. 1 as a function of p/p_{12} for four different pairs of governing parameters r_s and ρ. Here $p_{12}=\sqrt{2mE_{12}^{(0)}}$ is the momentum corresponding to the bare intersubband energy gap $E_{12}^{(0)}$. The values of these governing parameters in our computations are $\{r_s,\rho\}=\{0.7,1.35\}$, $\{1.06,3.13\}$, $\{1.69,7.85\}$, and $\{2.17,3.46\}$. These values completely define all dimensionless characteristics of the system. Note that the first three cases correspond to the same bare intersubband gap, where $E_{12}^{(0)}\propto\rho/r_s^2=\text{const}$. We have chosen $\rho>1$ in all four cases, which means that the Fermi level lies below the excited subband (the interaction only increases the final "dressed" intersubband gap, as we will see below in Fig. 2). Hence the population of second subband is small at zero temperature, $n_2(p)\sim 10^{-3}$, as we see in Fig. 1. The dependence $n_1(p)$ has an expected shape for a normal (Landau-type) Fermi fluid at $T=0$ with a discontinuity at the Fermi momentum p_F and a smooth dependence elsewhere. In contrast, the electron momentum distributions in the excited subband are smooth everywhere, as expected.

The Fermi momentum p_F is completely defined by the position of the discontinuity in $n_1(p)$ in Fig. 1. On the other hand, it is an exact statement of the Landau Fermi-liquid theory that (in a 2D case) that $n=p_F^2/2\pi$. This is a nontrivial fundamental relation and an independent condition that we checked numerically to be valid within the expected accuracy (margin of error less than 1% for all $\{r_s,\rho\}$ considered). This compliance is not accidental: the general theory by Baym[30] shows that all so-called conserving approximations,

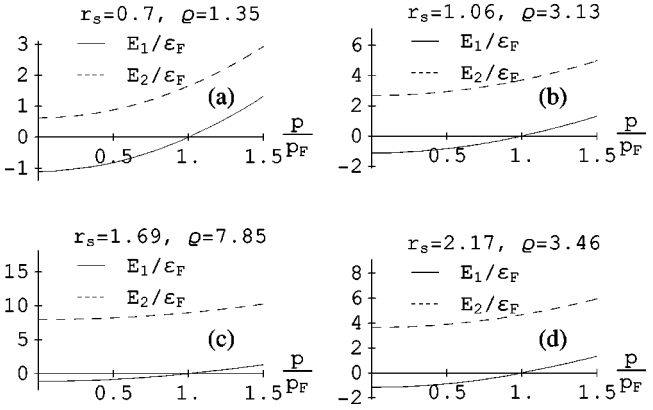

FIG. 2. Quasiparticle dispersion curves for the first and second subbands, $E_1(p)$ and $E_2(p)$, are plotted for the four different values of pairs $\{r_s,\rho\}$ indicated in the figure.

among them the SCRPA (GW approximation), automatically satisfy this fundamental relation. Note that the conventional (non-self-consistent) RPA (G_0W_0 approximation) is not conserving: it does not conserve the number of particles (in the presence of a weak probe field) and, consequently, does not satisfy this fundamental relation.[31]

Another quantity of interest is the quasiparticle spectrum in each subband. The quasiparticle energy for a subband is defined as the solution of the equation

$$E_i(\mathbf{p})=E_{i,\mathbf{p}}^{(0)}-\mu+\mathrm{Re}\Sigma_i^r[\mathbf{p},E_i(\mathbf{p})]. \tag{32}$$

The quasiparticle dispersion curves for both subbands are shown in Fig. 2 for the four values of the parameter pairs used in the computations, as indicated in the figure. As one can see, these curves for the first and second subbands are somewhat nonparallel, reducing the transition energy for larger momenta. This effect leads, in particular, to a broadening of the intersubband absorption spectra (cf. Sec. IV B). Another interesting effect is the widening of the intersubband spectral gap $E_{12}\equiv E_2(\mathbf{p}=\mathbf{0})-E_1(\mathbf{p}=\mathbf{0})$ due to the interaction. For the parameters of Figs. 2(a)–2(d), the relative change of E_{12} with respect to the Fermi energy is calculated to be $(E_{12}-E_{12}^{(0)})/\varepsilon_F=0.31$, 0.59, 1.14, and 1.25. This increase of the relative shift with r_s is an expected consequence of the screening that becomes less efficient at lower electron densities. A less obvious effect is that the *absolute* shift still decreases with increase of r_s (i.e., with decrease of the electron density), as one can easily verify.

To discuss these dispersion curves, the ground subband energy (in the units of the Fermi energy) $E_1(p)/\varepsilon_F$ at $p=0$ in Fig. 2 is less than -1 [by convention, $E_1(p_F)=0$]. This means that the ground-subband quasiparticle energies inside the Fermi sphere are lowered relative to those of noninteracting electrons due to the electron correlations taken into account by the SCRPA. This effect is closely related to the decrease of the total energy of the system when the correlations between the electrons are taken into account. Such a decrease of the total energy when "good" (correlated) electron wave functions are used is expected from the general variational principle. It can also be considered as analogous

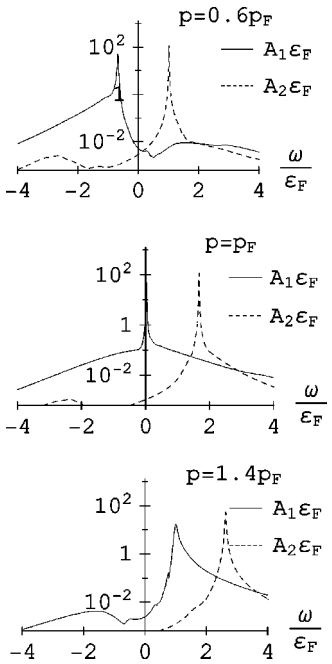

FIG. 3. Scaled spectral functions of the system for the first and second subbands, $\varepsilon_F A_1(\mathbf{p},\omega)$ and $\varepsilon_F A_2(\mathbf{p},\omega)$, found in the SCRPA, are plotted against the relative frequency ω/ε_F for $\{r_s,\rho\}=\{0.7,1.35\}$ and the values of momentum p indicated. Note the logarithmic scale.

to the decrease of the total energy and lowering of the one-electron energies for occupied orbitals when a molecule is formed from atoms. The fact that the SCRPA correctly reproduces this lowering of the one-electron energies inside the Fermi sphere indicates that it better describes the correlated many-electron state. Note that the one-electron energy in the excited subband is increased due to the electron correlations, as may be deduced from the data of Fig. 2. These effects bring about an increase of the intersubband transition energy $E_{12}(p)=E_2(p)-E_1(p)$, which is one of the causes of the blueshift of the intersubband absorption contour (see below in Sec. IV B).

The maximum information on one-electron quantities is contained in the spectral functions of the system:[32]

$$A_i(\mathbf{p},\omega)=-2\ \mathrm{Im}\ G_i^r(\mathbf{p},\omega). \tag{33}$$

These functions satisfy a sum rule

$$\int \frac{d\omega}{2\pi} A_i(\mathbf{p},\omega)=1. \tag{34}$$

This sum rule is a nontrivial condition that we have used to check the numerical accuracy of our results. It has been satisfied with an error not exceeding 1%, as expected.

Spectral functions $A_1(\mathbf{p},\omega)$ and $A_2(\mathbf{p},\omega)$ are plotted in Fig. 3 against the relative frequency for $\{r_s,\rho\}=\{0.7,1.35\}$ and selected values of momentum p. As we can see, these spectral functions at a given p have sharp peaks at the corresponding quasiparticle energies (measured from the chemical potential) $E_i(p)$ defined in Eq. (32). Note that for $p=p_F$, the spectral function of the first subband A_1 contains a

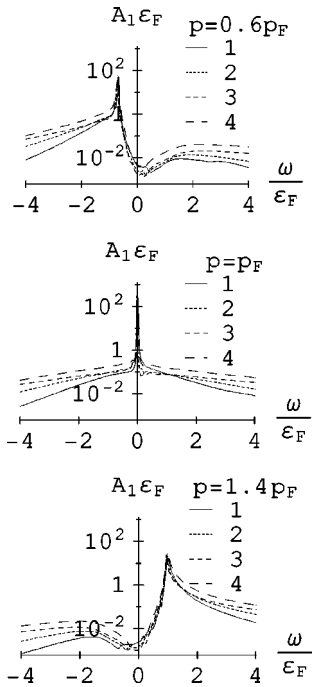

FIG. 4. Scaled spectral functions plotted against relative frequency ω/ε_F for the values of momentum p indicated. Curves 1–3 are plotted for relative spectral function of the first subband $\varepsilon_F A_1(p,\omega)$ for three parameter pairs $\{r_s,\rho\}=\{0.7,1.35\}$, $\{1.06,3.13\}$, and $\{1.69,7.85\}$, respectively. Curve 4, adopted from Ref. 24 and shown for comparison, corresponds to the scaled spectral function $\varepsilon_F A(p,\omega)$ for a pure 2D electron gas with $r_s=1.16$.

δ-function peak at $\omega=0$, while the spectral function for the excited subband does not have a δ-function singularity since it actually corresponds to electrons above the Fermi surface. Numerically, the δ-function peak has a very small width introduced for the regularization required by the computational procedures through a small negative addition to $\mathrm{Im}\Sigma^r$ for a narrow region around $\omega=0$.

Interesting scaling properties of the spectral functions can be traced in Fig. 4 where we show the scaled spectral functions for the first subband, $\varepsilon_F A_1(p,\omega)$, for three values of the parameter pairs $\{r_s,\rho\}=\{0.7,1.35\}$, $\{1.06,3.13\}$, and $\{1.69,7.85\}$ (curves 1–3). As curve 4, we show a scaled spectral function $\varepsilon_F A(p,\omega)$ for a 2D electron gas with $r_s=1.16$ adopted from our previous work,[24] which formally corresponds to $\{r_s,\rho\}=\{1.16,\infty\}$. As we see from this figure, in the vicinity of the quasiparticle peak, the scaled quantity $\varepsilon_F A_1$ is with a good accuracy a *universal* function of ω/ε_F. Though this universal behavior is not yet understood analytically, it is very pronounced: the curves in Fig. 4 corresponding to the same p/p_F practically coincide for different $\{r_s,\rho\}$. The deviation from this universal behavior is seen only for far wings where the spectral function itself is small. Note that a similar universality for the 2D case was discovered in Ref. 24.

B. Optical absorption results

We define normalized (dimensionless) absorption function $\tilde{\alpha}(\omega)$ by a relation

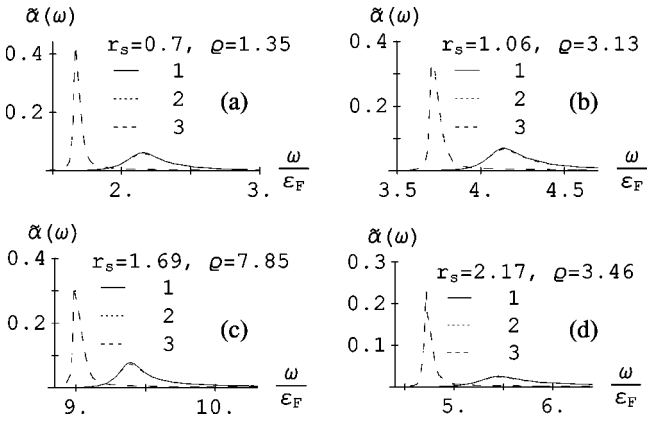

FIG. 5. The normalized intersubband absorption function $\tilde{\alpha}(\omega)$ calculated in the SCRPA approximation plotted as a function of the relative frequency ω/ε_F for different values of parameter pairs $\{r_s,\rho\}$ indicated. Curve 1 is for both the depolarization effect and vertex corrections taken into account, curve 2 includes only the depolarization effect, and curve 3 is calculated disregarding both the depolarization effect and vertex corrections (see the text for details).

$$\tilde{\alpha}(\omega)=\alpha(\omega)L\sqrt{\epsilon_b}, \tag{35}$$

where $L=V/S$ is the length (in the growth direction) of the system per a quantum well. This function $\tilde{\alpha}(\omega)$ depends only on the two parameters of the system: r_s and ρ.

The normalized absorption function $\tilde{\alpha}(\omega)$ is shown in Fig. 5 in three different approximations for different values of $\{r_s,\rho\}$ parameters as a function of relative frequency ω/ε_F. Curve 1 denotes the complete result with the depolarization shift and vertex corrections as given by Eq. (25) and the subsequent equations in Sec. II B. Curve 2 is computed without the vertex corrections, i.e., setting $\Gamma(\mathbf{p},\omega+\omega',\omega')=1$ in Eq. (28). Furthermore, curve 3 is calculated without the vertex corrections or depolarization effect, which additionally implies setting $V_x(\mathbf{q})=0$ in Eq. (26).

As one can see from Fig. 5, the depolarization effect, which is described by the denominator on the right-hand side of Eq. (26), dramatically affects the absorption function (cf. curves 2 and 3): in its presence, the absorption contour (curve 2) is approximately four times lower and significantly blueshifted compared with that in the absence of the depolarization effect (curve 3). The absorption contour (curves 1 and 2) is also significantly broadened due to the depolarization effect. This broadening can be traced to the finite width of the spectral function, and physically is due to electrons off the Fermi surface that experience efficient Coulomb scattering. We emphasize that this broadening of the absorption contour is obtained self-consistently within the microscopic theory and is not introduced phenomenologically. Unlike the depolarization effect, the vertex corrections have a small influence on the absorption (cf. curves 1 and 2). Note that in the absence of the depolarization effect (curve 3), the maximum of the absorption peak in frequency closely corresponds to the dressed intersubband separation E_{12}.

In the usual (non-self-consistent) RPA, where the polarization operator is defined by the bare Green's functions as $\Pi=G_0G_0$, the absorption spectrum has the form of a δ-function peak. The frequency of the absorption peak in the RPA was given by Ando and co-workers[26,27] as

$$\omega_m^{\mathrm{RPA}}=E_{12}^{(0)}\left(1+\frac{8\pi e^2 n}{\epsilon_b E_{12}^{(0)}}\int_{-\infty}^{\infty}dz\left[\int_{-\infty}^{z}dz'\,\phi_1(z')\phi_2(z')\right]^2\right)^{1/2}. \tag{36}$$

The corresponding depolarization shift in the RPA of this peak is $\Delta\omega_m^{\mathrm{RPA}}=\omega_m^{\mathrm{RPA}}-E_{12}^{(0)}$.

TABLE I. Absorption peak position ω_m, its depolarization shift $\Delta\omega_m$, and the bare intersubband gap $E_{12}^{(0)}$ in the units of the Fermi energy ε_F. The data are shown for the four cases of parameters r_s and $\rho=E_{12}^{(0)}/\varepsilon_F$, corresponding to curves 1-4 in Fig. 1; the labels RPA and SCRPA indicate the corresponding approximation. For ω_m in the SCRPA, we include the depolarization shift and vertex corrections, while in the RPA we use Eq. (36).

	r_s	$\frac{E_{12}^{(0)}}{\varepsilon_F}$	RPA $\frac{\omega_m}{\varepsilon_F}$	SCRPA $\frac{\omega_m}{\varepsilon_F}$	RPA $\frac{\Delta\omega_m}{\varepsilon_F}$	SCRPA $\frac{\Delta\omega_m}{\varepsilon_F}$
1	0.70	1.35	1.80	2.15	0.45	0.49
2	1.06	3.13	3.61	4.14	0.48	0.43
3	1.69	7.85	8.36	9.40	0.50	0.40
4	2.17	3.46	4.36	5.45	0.89	0.73

In Table I we summarize the position of the absorption maxima, ω_m, in the SCRPA and RPA along with the corresponding shifts of the absorption maxima, $\Delta\omega_m$, due to the depolarization effect. For SCRPA this shift is defined as the difference between the coresponding maximum of the absorption spectrum $\omega_m^{\mathrm{SCRPA}}$ and the (renormalized) intersubband spectral gap E_{12} [see below Eq. (32)]: $\omega_m^{\mathrm{SCRPA}}=\omega_m^{\mathrm{SCRPA}}-E_{12}$. As we can conclude from this table, there is a blueshift of absorption maximum frequency in RPA with respect to the bare intersubband gap, as is known,[26] and also a significant further blueshift of the absorption in the SCRPA with respect to the RPA. To pinpoint the origin of this blueshift, we note from Table I that the depolarization shifts in the SCRPA and RPA, though significant, do not differ much. Therefore, the blueshift of the SCRPA with respect to the RPA is mostly due to the widened intersubband gap (cf. Fig. 2) and not due to an increase of the depolarization shift in the SCRPA.

It is of considerable interest to compare our theory with experimental data. There exists a significant amount of experimental data for the intersubband optical absorption in quantum wells (some of such data is reviewed in Ref. 33). However, keeping in mind the high application potential of quantum-well infrared photodetectors (QWIP's), we have chosen to concentrate on the data of Refs. 34 and 35, where QWIP's were explored. In performing the corresponding calculations, we modified the computational code to take into account the finite heights of the barriers in QWIP's. Correspondingly, the well energies and wave functions were modified with respect to the infinite-barrier values of Eq. (31).

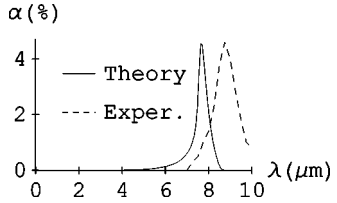

FIG. 6. Optical absorbance spectra of electrons for a QWIP with 32 individual quantum wells vs the light wavelength. Solid curve: theory; dashed curve: experiment (Ref. 34). The computations are done for the experimental conditions: (Ref. 34) *P* polarization at the Brewster angle.

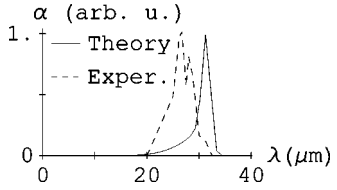

FIG. 7. Computed optical absorption spectrum in comparison with the experimental responsivity of the QWIP of Ref. 35. Both the quantities are plotted in arbitrary units and are normalized to the maximum value of 1. Solid curve: theory; dashed curve: experiment (Ref. 35).

Starting the discussion with the earlier paper,[34] the density of the electron gas (created by a δ doping of the quantum wells) $n \approx 9 \times 10^{11}$ cm^{-2}, corresponding to $r_s \approx 0.6$, is well within our convergence range (cf. Fig. 1 in Ref. 24). The barrier/well composition is $Al_{0.27}Ga_{0.73}As/GaAs$, the well width is 6 nm, and the barrier width is 25 nm. Note that under these conditions, the first excited one-electron level is at 204 meV, just 15 meV below the barrier top, as deliberately designed for the photodetector functioning.

We have calculated the electron absorption spectrum for 30 individual quantum wells in a multiple-quantum-well heterostructure for the above indicated parameters of Ref. 34, except that we have considered the electron-donor dopants as being uniformly distributed inside the quantum well to simplify the computations. The obtained result is displayed in Fig. 6 in comparison with the corresponding experimental absorption spectrum (see Fig. 2 of Ref. 34). Note that both the shape of the absorption contour and the magnitude of the absorption have been calculated and should be compared. We emphasize that *our theory does not contain any adjustable parameters*. The most important result of our computations is that the calculated absorption spectrum has a significant width, comparable to that of the experimental spectrum. This width is due to the electron-electron interactions that are consistently taken into account in the SCRPA (GW approximation), causing the finite lifetimes of the quasiparticles off the Fermi surface, which is also reflected in the width of the spectral function peaks (cf. Figs. 2 and 3). In contrast, the ordinary RPA (G_0W_0 approximation) does not result in any finite spectral widths at zero temperature. Note that the experimental spectrum is still somewhat wider than the theoretical one, which suggests that there are other sources of the broadening, one of them being the nanoroughness of the quantum-well/barrier interface.

Another important characteristic, the magnitude of the maximum absorption in Fig. 6, is in an almost perfect agreement with the experiment, but we do not want to overemphasize this fact. The position of the calculated spectral maximum is blueshifted by $\approx 12\%$. The origin of this shift is presently not identified. Different factors may contribute to it. One of them is the already mentioned well-interface roughness. The second factor may be the δ doping of the well, which is difficult to take into account computationally. Yet another factor is our two-subband approximation, which is necessary due to the computational complexity. Finally, a factor contributing to this shift may be the approximate nature of the present theory both in the treating of the electron-electron interactions and the neglect of the electron-phonon interactions.

The second of the experimental papers with which we compare, (Ref. 35), dealt with a QWIP consisting of 20 periods of GaAs quantum wells of 11.8-nm width, each separated by 40-nm $Al_{0.07}Ga_{0.93}As$ barriers. The quantum wells are doped to the electron density of 4.7×10^{10} cm^{-2} corresponding to $r_s \approx 2.6$. This value is close to the boundary of the region of convergence of our numerical procedure, but still is inside that region (cf. Fig. 1 in Ref. 24). The absorption spectrum was not explicitly measured in Ref. 35, but we know from Ref. 34 that the line shapes of the optical absorption and the QWIP responsivity are quite similar. Based on this, in Fig. 7 we compare our computed absorption spectrum with the responsivity spectrum of Ref. 35. In such an evaluation, we are, indeed, able to compare only the corresponding lineshapes, but not the magnitudes.

The comparison of the computed and experimental curves in Fig. 7 shows that in this case the computed width of the absorption contour is significant, though appreciably (about twice) smaller than that of the experimental curve. The shape of the experimental spectrum is significantly different featuring a dip at ≈ 27.8 nm that is attributed to the absorption of TO+TA phonons.[35] It is interesting to note that in this case the theoretical contour is *redshifted* with respect to the experimental one in contrast to Fig. 6, where there is a blueshift. Same possible reasons of the distinctions between the theory and experiment apply as mentioned in the discussion of Fig. 6 above.

V. CONCLUDING REMARKS

We have found equilibrium Green's functions and related one-electron properties and the intersubband absorption function for a system of electrons with Coulomb interaction bound in a quantum well with two subbands. We have employed the self-consistent random phase approximation (SCRPA) in the framework of the Kadanoff-Baym-Keldysh (KBK) Green's-function method. This approach, in principle, allows one to describe a system at a given arbitrary temperature, though in this paper it has been natural to limit ourselves to the case of zero temperatures. We have used an iterative method[24] of solving the highly nonlinear field-theoretical equations, which is stable, convergent, and efficient in a wide enough region of electron densities.

For the future studies of laser-induced ultrafast kinetics of

electrons in quantum wells, the present paper is a useful preliminary investigation where the initial correlated state of the electron system to be considered kinetically is found. Note that previous investigations in quantum kinetics of electrons did not use such a microscopically found initial state. In the intersubband-transition model, noncorrelated electrons were used as the initial state.[5,8–10] Another approach[7] used relaxation from a uncorrelated, nonstationary state leading to a stationary correlated state that was then employed as the initial state for quantum kinetics. A drawback of this method of preparing a stationary correlated state is the impossibility to obtain a predetermined temperature, in particular, the zero temperature. We note that there exists a method of imaginary time stepping[36] that also allows one to build a correlated self-consistent Green's functions. This method was implemented for nuclear collisions in Ref. 37 using the generalized Kadanoff-Baym ansatz. This imaginary time-stepping method requires both iterations to achieve self-consistency and a solution of the temporal equations and is, in principle, equivalent to our approach.

There is also another prospective application of the present theory to ultrafast processes. The *linear* reaction of any system to an electromagnetic field that has arbitrary temporal dynamics, but is weak in the magnitude, is determined through the well-known Kubo theory by the many-body Green's functions of the *equilibrium* system. In particular, the computation of the corresponding ultrafast polarization will require only a Fourier transform of the corresponding current-current correlation function. Such a function is found in the present paper in the self-consistent random-phase approximation in Sec. II B. We will pursue this line of investigation elsewhere.

There has been an important discussion regarding the longitudinal *f*-sum rule and its relation to the local conservation laws for Green's functions.[38–40] This sum rule is formulated for the renormalized Coulomb line $W(\mathbf{p},\omega)$ that is a building block of the theory. It was shown[21] that the SCRPA (called a shielded approximation in Ref. 21) is a conserving theory where the local conservation laws (for current, momentum, etc.) are satisfied. However, it is known that $W(\mathbf{p},\omega)$ in the SCRPA does not fulfill the *f*-sum rule. It was argued[39] that adding Coulomb lines inside the polarization operator would significantly improve the agreement with the *f*-sum rule. However, such a modification brings about a violation of the local conservation laws.[40] In particular, such a violation would completely preclude the use of the obtained solutions for the description of the initial state for quantum kinetics problems. The cause of this violation is that the theory of Ref. 39 is incompatible with the general method of constructing conserving theories by Baym and Kadanoff.[21] In this connection, we note that a numerically solvable approximate theory that would simultaneously satisfy the Baym-Kadanoff conservation conditions and the *f*-sum rule has not been developed so far.

An approach to this general problem was given in Ref. 21). In the framework of this approach, the Green's functions were obtained in a conserving theory (SCRPA, in particular). After that, a modified Coulomb line $W(\mathbf{p},\omega)$ was calculated using these Green's functions by solving the Bethe-Salpeter equation. Such a quantity will exactly satisfy the *f*-sum rule.[21,40] However, it is important to bear in mind that such a modified (''improved'') Coulomb line cannot be used as a building block for the next generation of self-consistent Green's functions, because the resulting theory would not fit the framework of Ref. 21 and therefore generally would not be conserving.

Without repeating the detailed discussion of the results obtained given in Secs. IV A and IV B, let us briefly mention what we consider to be the main results of the paper. We have generalized the method of Ref. 24 from a 2D electron gas to electrons confined in a quantum well with two subbands (potentially, many subbands can be included in the future). The Green's functions found bear the maximum information on the one-electron properties of the system (momentum distribution, electron dispersion and lifetimes, etc.). That has allowed us, in particular, to find the intersubband optical absorption whose spectral contour is significantly blueshifted with respect to the conventional (non-self-consistent) RPA and acquires a finite width due to electron-electron scattering. Most of this blueshift is caused by the significant increase of the intersubband separation due to the electron correlations. An additional significant blueshift is caused by the depolarization effect. In contrast, the effect of vertex corrections in the ladder approximation is small albeit noticeable.

A wide area of applications of the results obtained will be the description of the intersubband optical absorption in numerous infrared electro-optical devices, in particular, QWIP's.[34,35] The theory of such devices was previously mainly based on phenomenological or semiphenomenological formulas. We have shown that the present theory explains most of the spectral width of the optical responses in QWIP's and gives reasonable results for the position (with en error ~ 12–$15\,\%$) and spectral shapes of such responses *without any adjustable parameters*. Another potential application will be the use of the equilibrium Green's functions obtained in the present study in the capacity of the initial conditions for the quantum kinetics problems of electrons in quantum wells undergoing intersubband excitation.

ACKNOWLEDGMENTS

This work was supported by the Chemical Sciences, Biosciences and Geosciences Division of the Office of Basic Energy Sciences, Office of Science, U.S. Department of Energy. We appreciate useful discussions with S. G. Matsik and A. G. U. Perera.

*To whom correspondence should be addressed. Email address: mstockman@gsu.edu; web site: www.phy-astr.gsu.edu/stockman

[1] *Semiconductor Quantum Wells and Superlattices for Long-Wavelength Infrared Photodetectors*, edited by M.O. Manasreh (Artech House, Boston, 1993).

[2] K.K. Choi, *The Physics of Quantum Well Infrared Photodetectors* (World Scientific, Singapore, 1997).

[3] *Handbook of Thin Film Devices*, handbook edited by M.H. Fran-

combe, Vol. 2: *Semiconductor Optical and Electro-Optical Devices*, edited by A.G.U. Perera and H.C. Liu (Academic, San Diego, 2000).
[4] J. Faist and F. Capasso, in Ref. 3, Chap. 7.
[5] H. Haug and A.-P. Jauho, *Quantum Kinetics in Transport and Optics of Semiconductors* (Springer, New York, 1996).
[6] R. Binder, H.S. Köhler, M. Bonitz, and N. Kwong, Phys. Rev. B **55**, 5110 (1997).
[7] N. Hang Kwong and M. Bonitz, Phys. Rev. Lett. **84**, 1768 (2000).
[8] N. Hang Kwong, M. Bonitz, R. Binder, and H.S. Köhler, Phys. Stat. Solidi B **206**, 197 (1998).
[9] L. Bányai, Q.T. Vu, B. Mieck, and H. Haug, Phys. Rev. Lett. **81**, 882 (1998).
[10] Q.T. Vu, L. Bányai, H. Haug, F.X. Camescasse, J.-P. Likforman, and A. Alexandrou, Phys. Rev. B **59**, 2760 (1999).
[11] P. Gartner, L. Banyai, and H. Haug, Phys. Rev. B **60**, 14 234 (1999).
[12] Q.T. Vu, H. Haug, W.A. Hügel, S. Chatterjee, and M. Wegener, Phys. Rev. Lett. **85**, 3508 (2000).
[13] M. Bonitz, in *Quantum Kinetic Theory* (Teubner, Stuttgart, 1998).
[14] L.P. Kadanoff and G. Baym, *Quantum Statistical Mechanics*, (Benjamin, New York, 1962).
[15] L.V. Keldysh, Zh. Éksp. Teor. Fiz. **47**, 1515 (1965) [Sov. Phys. JETP **20**, 1018 (1965)].
[16] D.C. Langreth, in *Advanced NATO Study Institute, Series B: Physics*, edited by J. T. Devreese and V. E. Van Doren (Plenum, New York, 1967), p. 3.
[17] J. Rammer and H. Smith, Rev. Mod. Phys. **58**, 323 (1986).
[18] A.A. Abrikosov, L.P. Gor'kov, and I.E. Dzyaloshinskii, *Quantum Field Theoretical Methods in Statistical Physics*, 2nd ed. (Pergamon, New York, 1965), Chap. 7.
[19] M. Lindberg and S. Koch, Phys. Rev. B **38**, 3342 (1988).
[20] G. Manzke and K. Henneberger, in *Progress in Nonequilibrium Green's Functions*, Edited by M. Bonitz, (World Scientific, Singapore, 2000), p. 238.
[21] G. Baym and L.P. Kadanoff, Phys. Rev. **124**, 287 (1961).
[22] U. von Barth and B. Holm, Phys. Rev. B **54**, 8411 (1996); **55**, 10 120(E) (1997).
[23] B. Holm and U. von Barth, Phys. Rev. B **57**, 2108 (1998).
[24] S.V. Faleev and M.I. Stockman, Phys. Rev. B **62**, 16 707 (2000).
[25] S.V. Faleev and M.I. Stockman, Phys. Rev. B **63**, 193302 (2001).
[26] T. Ando, Z. Phys. B: Condens. Matter **26**, 263 (1977).
[27] T. Ando, A.B. Fowler, and F. Stern, Rev. Mod. Phys. **54**, 437 (1982).
[28] D. Huang, G. Gumbs, and M.O. Manasreh, Phys. Rev. B **52**, 14 126 (1995).
[29] P. von Allmen, Phys. Rev. B **46**, 13 351 (1992).
[30] G. Baym, Phys. Rev. **127**, 1391 (1962).
[31] P. Garcia-Gonzales and R.W. Godby, Phys. Rev. B **63**, 075112 (2001).
[32] G.D. Mahan, *Many-Particle Physics* (Plenum, New York, 1990).
[33] T. Elsaesser, and M. Woerner, Phys. Rep. **321**, 253 (1999).
[34] A.G. Steele, H.C. Liu, M. Buchanan, and Z.R. Wasilewski, J. Appl. Phys. **72**, 1062 (1992).
[35] A.G.U. Perera, W.Z. Shen, S.G. Matsik, H.C. Liu, M. Buchanan, and W.J. Schaff, Appl. Phys. Lett. **72**, 1596 (1998).
[36] P. Danielewicz, Ann. Phys. (N.Y.) **152**, 239 (1984).
[37] H.S. Köhler, Phys. Rev. C **51**, 3232 (1995).
[38] W.-D. Schöne and A. Eguiluz, Phys. Rev. Lett. **81**, 1662 (1998).
[39] D. Tamme, R. Sheppe, and K. Henneberger, Phys. Rev. Lett. **83**, 241 (1999).
[40] A. Eguiluz, Phys. Rev. Lett. **83**, 242 (1999).